Comparative performance of high and medium resolution cameras for defect detection in carbon-fiber reinforced composites by digital shearography

Abedin, Kazi Monowar; Tao, Nan; Anisimov, Andrei G.; Groves, Roger M.

DOI
10.1117/12.2669718

Publication date
2023

Document Version
Final published version

Published in
Optical Measurement Systems for Industrial Inspection XIII

PROCEEDINGS OF SPIE

SPIEDigitalLibrary.org/conference-proceedings-of-spie

Comparative performance of high and medium resolution cameras for defect detection in carbon-fiber reinforced composites by digital shearography

Kazi Monowar Abedin, Nan Tao, Andrei Anisimov, Roger Groves

Kazi Monowar Abedin, Nan Tao, Andrei G. Anisimov, Roger M. Groves, "Comparative performance of high and medium resolution cameras for defect detection in carbon-fiber reinforced composites by digital shearography," Proc. SPIE 12618, Optical Measurement Systems for Industrial Inspection XIII, 126181X (15 August 2023); doi: 10.1117/12.2669718

SPIE.

Event: SPIE Optical Metrology, 2023, Munich, Germany

Comparative performance of high and medium resolution cameras for defect detection in carbon-fiber reinforced composites by digital shearography

Kazi Monowar Abedin*[a], Nan Tao[b], Andrei G. Anisimov[b], Roger M. Groves[b]
[a]Dept. of Physics, College of Science, Sultan Qaboos University, Al-Khodh, Muscat, 123 Oman;
[b]Department of Aerospace Structures and Materials, Delft University of Technology, Kluyverweg 1, 2629 HS, Delft, the Netherlands

ABSTRACT

The performance of defect detection in composite materials using digital shearography is important for correct decision-making in non-destructive testing. In this work, we compared a high-resolution 24-megapixel digital still camera (DSLR) and a conventional medium-resolution 5-megapixel camera to determine the detectability of blind holes in an aerospace-graded carbon-fiber reinforced polymer (CFRP) sample. The hole diameters ranged from 0.2 to 3 mm with a material thickness of 4 mm and the test sample dimensions of 200×200 mm. The sample was heated and observed from the front (defect-free side) by three halogen lamps for 5 minutes in pulsed heating mode. Speckle interferograms were acquired during the heating and cooling phases from both cameras simultaneously using identical shearing interferometers and shearing distances. Phase maps were calculated using the 4+4 temporal phase step algorithm and then unwrapped. Further, defect-induced deformation (DID) phase maps were obtained by polynomial curve fitting. The DID phase maps obtained from the two cameras were compared. Blind holes with diameters up to 1 mm were detected, which are one of the smallest defects detected with shearography and reported in literature. In addition, the DLSR camera was able to detect holes of 0.8 mm in diameter. We observed that nearly comparable detection capabilities were obtained from both cameras, even though the spatial resolution of the second camera (DLSR) was 5 times higher. Possible reasons of this limitation include effects such as fiber-related deformation in CFRP and speckle noise.

Keywords: digital shearography, nondestructive testing, composites, carbon-fiber reinforced polymer, thermal loading, high-resolution camera

1. INTRODUCTION

Carbon-fiber reinforced polymers (CFRP)[1,2] are extensively used both in aerospace and marine applications due to their higher strength and stiffness in combination with their light weight. Due to delamination and fiber breakage caused mainly by external stresses, the structural integrity of composites may degrade significantly[3]. Nondestructive testing (NDT) techniques are required to improve the safety and reliability of CFRP structures. NDT of thin composite structures employed in aerospace engineering has been studied extensively[4]. Among the various NDT methods available, shearography is an optical interferometric technique with the advantages of high-sensitivity to deformation changes, full-field observation capability, robustness to environmental disturbances, real-time results, and non-contact measurement. It directly measures the derivatives of surface deformation, which are closely related to surface strain components[5,6]. This allows shearography to inspect structures by looking for defect-induced anomalies in the surface strain field directly from the fringe pattern and/or phase maps.[7]

A vital procedure for shearography NDT is to load the test object during the inspection. Of the various loading techniques available, thermal loading has been used frequently[5,8]. Akbari *et al.*[9] studied the thermal loading parameters in a shearography test by using a numerical-experimental approach. As mentioned, even though applications for shearography NDT of thin composite materials were well discussed in the literature, an inspection of thicker composites has been conducted by relatively few researchers[10,11]. More recently, Tao *et.al* [12,13] have performed a numerical-experimental study on the defect detection capability in thick fiber-reinforced composite laminates. While it successfully detected defects in

*abedin@squ.edu.om; phone 968 9675-4971

Optical Measurement Systems for Industrial Inspection XIII, edited by Peter Lehmann,
Proc. of SPIE Vol. 12618, 126181X · © 2023 SPIE · 0277-786X
doi: 10.1117/12.2669718

thick materials, the size of detected defects (flat bottom holes) was relatively large (60 mm in diameter and 30 mm in depth)[12]. Following some of the recent developments for thick composites, this paper addresses defect detection capabilities in carbon-fiber reinforced composites with a thickness of 4 mm.

A possible way to increase the sensitivity of detection is by increasing the spatial resolution of the imaging device. If a higher-resolution imaging device is used, the detection sensitivity of the shearography could be improved, especially for smaller defects. Conventional video-rate cameras are limited to a maximum spatial resolution of about 6 Megapixels (MP)[5]. Recently high-resolution digital still cameras, having a resolution of up to 24 MP have been successfully employed in shearography[14,15] which resulted in improved spatial resolution in phase-shifting. It would be interesting to use these high-resolution cameras for non-destructive testing applications in shearography, particularly for the testing of composites with smaller defects. It would also be interesting to compare their performance with the medium-resolution cameras used in conventional shearography systems.

2. EXPERIMENTAL DETAILS

A set of blind holes was drilled in the reverse side of a 4 mm thick CFRP sample made from CYCOM 977-2 by Cytec with [0/90]s layup (Figure 1 (a)). The holes diameters ranged from 0.2 to 3 mm with depths from 1 to 3 mm (Figure 1 (b)). None of the holes reached the front side, and therefore, were hidden from view from the front side. It should be noted that the depth of the defects (blind holes) is defined in this paper as the remaining thickness of the material after drilling and not the depth of the blind holes. Also, these holes were drilled with conventional drills (cone of 135 deg), so these are not strictly the flat bottom holes that are often used as reference defects for non-destructive testing[4,12,13].

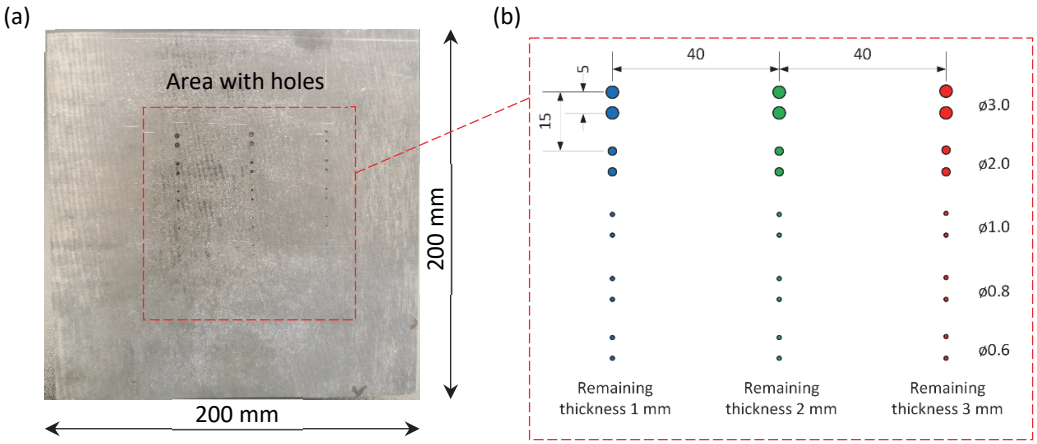

Figure 1. Photograph (a) and sketch (b) of the CFRP specimen with blind holes.
Units in mm. Note, ø3.0 refers to holes with a diameter of 3 mm.

The CFRP specimen was inspected by a modified 3D shape shearography instrument[16] from the opposite (front) side of the holes in an attempt to detect their presence (Figure 2). One mirror of the Michelson interferometer (Figure 2 (a)) was tilted by a fixed amount to impart a given amount of shear (dx, about 3.5 mm in the horizontal direction) to the two speckled images reflected from the two mirrors of the interferometer. Each camera has its interferometer with identical optics mounted adjacent to it with an equal amount of shear. A Nikon D3500 single-lens reflex camera (DSLR) camera with a 24 MP sensor was used as the high-resolution imaging device and a 5 MP machine vision video camera (Basler Pilot piA2400) was used as the medium-resolution camera. Both cameras had the same aperture of *f/8*, however different lenses were used: Nikon 18-55mm f/3.5-5.6 (set at 55 mm) with the DSLR camera, Linos MeVis-C 1.6/25 with the Basler camera.

The DSLR camera with the shearing interferometer was mounted above the medium-resolution camera (Figure 2 (b)). The specimen was illuminated by a Torus laser by Laser Quantum with about 200 mW of power at a wavelength of 532 nm. The field of view (FOV) of both cameras was approximately 200×200 mm, however, the resultant phase maps were cropped to exclude the specimen clamping region.

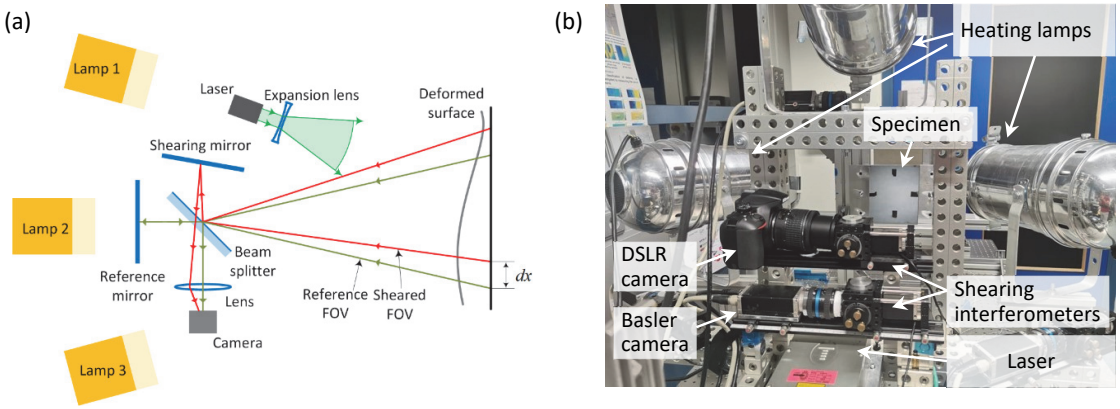

Figure 2. Shearography scheme and the instrument. (a) schematic of one shearing camera with the Michelson interferometer (both cameras had identical shearing interferometers; field of view (FOV), the shear distance dx), (b) modified 3D shape shearography instrument with the DSLR camera.

The specimen was heated from the front (defect-free) side by three 1000 W halogen lamps for approximately 5 minutes in a pulsed heating mode. Each heating cycle included 30 s of heating with the lamps on and 10 s with the lamps off to capture the interferograms. During these 10 s pauses and further in the cooling, the well-known 4+4 temporal phase stepping algorithm[5,6] was used to acquire the phase maps. The temporal phase-shifting was realised by piezo-electric actuators PSH 4z by Piezosystem Jena. As a result, sets of interferograms were captured by both cameras before the heating (reference state), during the heating pauses (after every 30 s heating cycle) and during cooling (every 60 s during 13 seconds of cooling; the frequency of measurement of 60 s was selected to result in a rational amount of data).

3. RESULTS

All phase-shifted sets of interferograms were processed to obtain shearography phase maps. The sequential approach was used, where phase change from neighbour data sets in time was calculated and then summed up with all phase changes obtained during heating and cooling. This was done for phase maps obtained with each camera independently. The processing of phase changes included the following steps:

Step 1. Spatial filtering with sin/cos averaging filter with the minimal aperture of 3x3 pixels to preserve the spatial resolution.

Step 2. 2D unwrapping to resolve phase jumps outside the range of [0, 2π].

Step 3. Compensation: defect-induced deformation (DID) phase maps were obtained by a polynomial surface fitting of the phase maps to exclude the phase change due to rigid body motion, bending and local deformation of the specimen.

The total phase maps before the compensation (excluding step 3) for both cameras are presented in Figure 3 (a, b). These phase maps are a direct sum of phase changes over 8 heating cycles (of 30 s each) and during 8 minutes of cooling. Further, each phase change was compensated to reveal the DID and contributed to the total sum of DID (Figure 3 (c,d)).

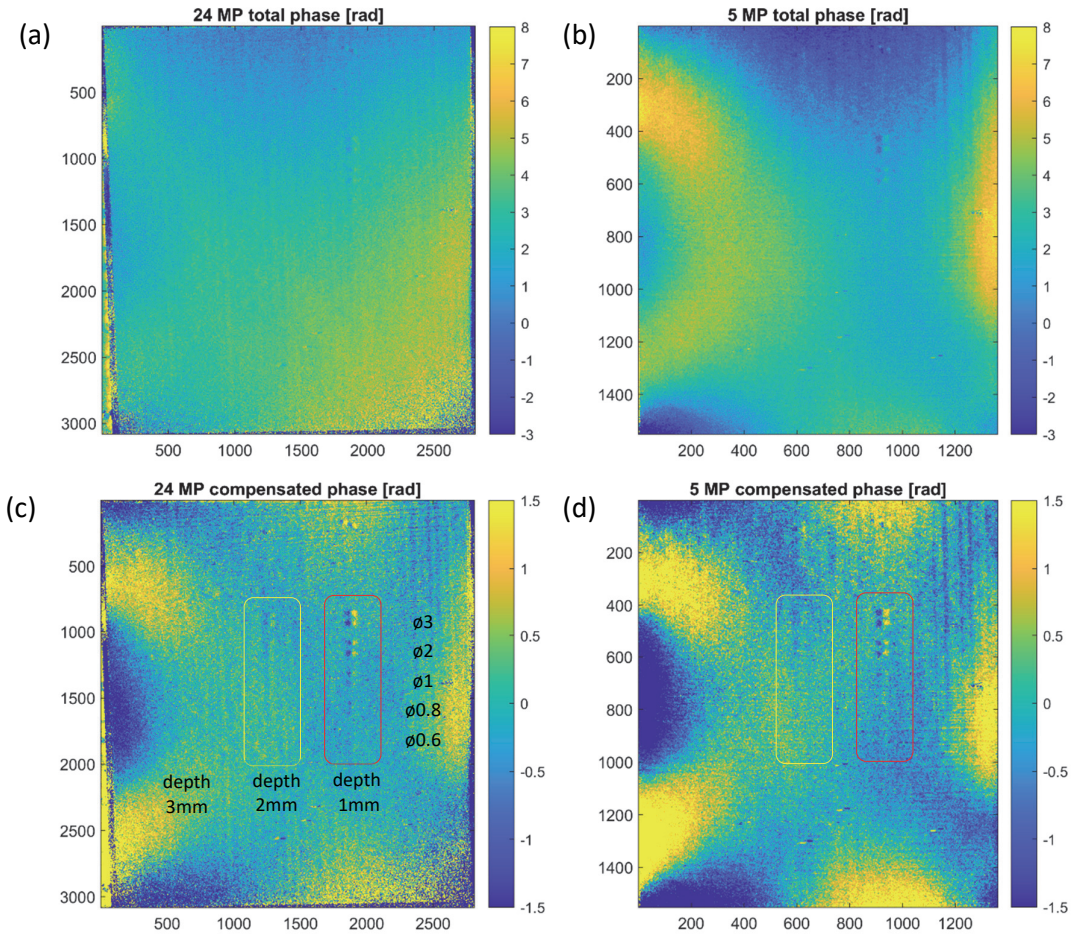

Figure 3. Shearography phase maps: (a, b) the total phase maps for 24 MP DSLR and 5 MP machine vision cameras, (c,d) corresponding compensated phase maps. Dimension units in pixels, phase units in radians

From Figure 3 (c,d) pairs of blind holes of ø3, ø2 with the depth (remaining thickness) of 1 mm in the red area and ø3 at 2 mm depth (yellow area) can be detected in phase maps from both cameras. Holes of ø1, ø0.8 mm at 1 mm depth and ø2 mm at 2 mm depth are barely detected. All holes at 3 mm depth (left part to the yellow) are not detected.

Figure 4 (a,c) zooms into the area with blind holes at 1 mm depth with the corresponding cross sections (Figure 4 (b, d)). According to these results, ø1 and 0.8 mm holes at 1 mm depth have better visibility in the phase map from 24 MP DSLR camera. The 0.8 mm hole was probably detected by the 24 MP DSLR camera only (see Figure 3 (c,d)).

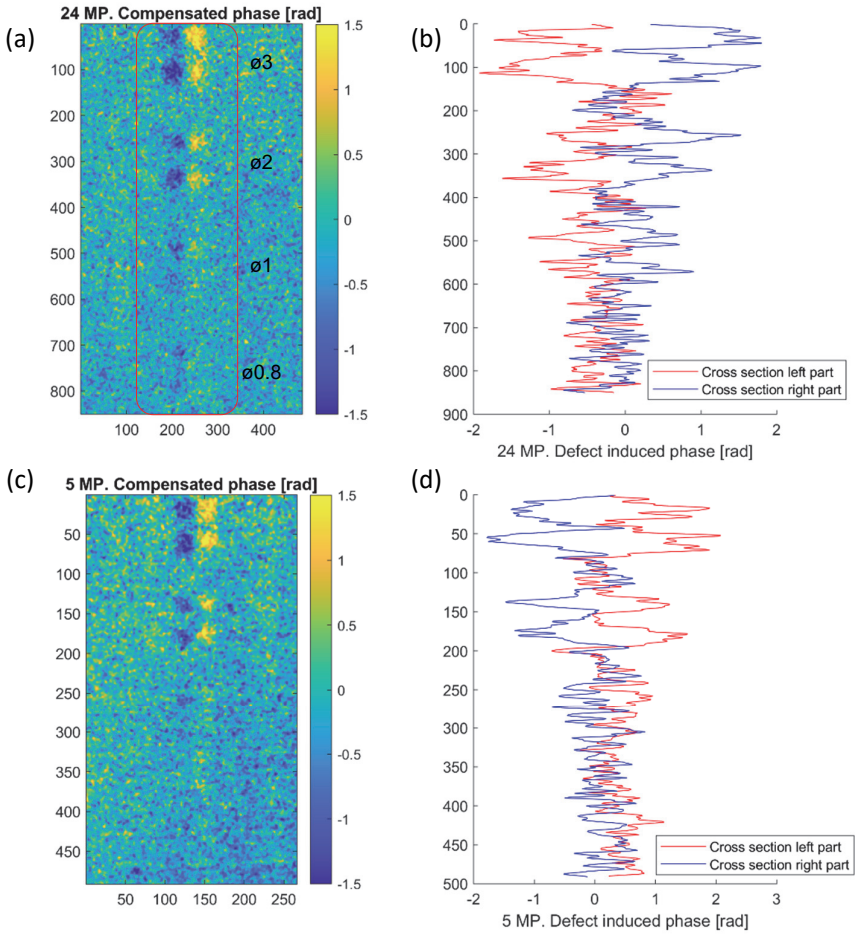

Figure 4. (a,b) Zoom into the defects at 1 mm depth (remaining thickness),
(c, d) corresponding cross sections along the columns with the signals from the blind holes.
Dimension units in pixels, phase units in radians

4. DISCUSSION

The differences in the total phase maps (Figure 3 (a, b)) on the left and right sides can be explained by an effective difference in the shear distances between two interferometers and a difference in the cameras orientation. The DSLR camera was located above the machine vision camera, effectively at a slightly different angle to the specimen surface which introduces the difference in the sensitivity vectors of both cameras.

Defects up to ø1 mm at 1 mm depth can be detected in the phase maps from both cameras. The DSLR camera also enables detection of ø0.8 mm at 1 mm depth.

The compensated phase maps (Figure 4) have a relatively high noise. One of the explanations may be a relatively slow phase-shifting procedure which took 10 s to record 4 interferograms. Additional delays were introduced to allow the DSLR camera to capture the frames. Such a long time for phase shifting with transient loading may cause additional noise and errors in phase reconstruction.

To sum up, the performance of the DLSR camera, which had about 5 times the pixel resolution of the machine vision camera fell short of the expectations. There may be additional reasons which are not well understood at present, such as

fiber-related deformation in CFRP and speckle noise, which prevented the full spatial resolution of the DSLR camera from being fully utilized.

5. CONCLUSION

We compared the performance of two cameras, one high-resolution DSLR 24 MP and the other medium resolution 5 MP machine vision, in detecting small-diameter blind holes in CRFP composite material. Blind holes of diameters down to 1 mm (0.8 mm for the DSLR camera) were detected, which are one of the smallest defects detected with shearography and reported in the literature. Comparable detection capabilities were obtained from both cameras, even though the spatial resolution of the DLSR camera was about 5 times higher. The reasons for this limitation are not well-understood at this point and more work is needed to explore the possible benefits of DSLR cameras in digital shearography.

ACKNOWLEDGEMENTS

KMA wishes to acknowledge the financial support provided by the Internal Grant (IG) project (#IG/SCI/PHYS/21/1) of Sultan Qaboos University.

This research was supported by the Operationeel Programma Zuid-Nederland (Op–Zuid) Project as part of the Dutch Composite Maintenance Centre (DCMC), supported by the Europees Fonds voor Regionale Ontwikkeling (EFRO) and the North Brabant province of the Netherlands.

This publication is based upon work from COST Action CA21155 – Advanced Composites under HIgh STRAin raTEs loading: a route to certification-by-analysis (HISTRATE), supported by COST (European Cooperation in Science and Technology).

REFERENCES

[1] Mouritz A.P., Gellert E., Burchill P. and Challis K., "Review of advanced composite structures for naval ships and submarines," Compos Struct 53, 21–42 (2001).
[2] Groves R.M., Inspection and Monitoring of Composite Aircraft Structures. In: Beaumont PWR, Zweben CH, editors. Compr. Compos. Mater. II, Oxford: Elsevier; p. 300–11 (2018).
[3] Montanini R. and Freni F., "Non-destructive evaluation of thick glass fiber-reinforced composites by means of optically excited lock-in thermography," Compos. - A: Appl. Sci. Manuf. 43, 2075–82 (2012).
[4] Ibrahim M.E., "Nondestructive evaluation of thick-section composites and sandwich structures: a review, " Compos Part A Appl Sci Manuf 64, 36–48 (2014).
[5] Yang L. and Xie X. Digital Shearography: New Developments and Applications. Bellingham: SPIE Press (2016).
[6] Francis, D.R., Tatam, R.P. and Groves, R.M., "Shearography technology and applications: a review," Meas. Sci. Technol., 21, 102001 (2010).
[7] Hung Y.Y., "Shearography for non-destructive evaluation of composite structures," Opt Lasers Eng 24 161-82 (1996).
[8] Liu Z., Gao J., Xie H. and Wallace P., "NDT capability of digital shearography for different materials", Opt Lasers Eng. 49, 1462–9 (2011).
[9] Akbari D., Soltani N. and Farahani M., "Numerical and experimental investigation of defect detection in polymer materials by means of digital shearography with thermal loading," Proc Inst Mech Eng Part B J Eng Manuf 227, 430–42 (2013).
[10] Murri W.J., Sermon B.W., Andersen R.N., Martinez L.A., der Heiden E.J. and Garner C.A., "Defects in thick composites and some methods to locate them." In: Thompson D.O., Chimenti D.E., editors. Rev. Prog. Quant. Nondestruct. Eval. Vol. 10B, Boston, MA: Springer US; p. 1583–90 (1991).
[11] di Scalea F.L., Spicer J.B. and Green R.E., "Electronic shearography with thermal loading for detecting debonds in thick polyurethane/ steel panels for marine applications," Res Nondestruct Eval 12, 43–51 (2000).
[12] Tao N., Anisimov A.G. and Groves R.M. "Shearography non-destructive testing of thick GFRP laminates: Numerical and experimental study on defect detection with thermal loading," Comp. Struc, 282, 11500 (2022).

[13] Tao N., Anisimov A.G. and Groves R.M., "FEM-assisted shearography with spatially modulated heating for non-destructive testing of thick composites with deep defects," Comp. Struc, 297, 1155980 (2022).
[14] Al Jabri, A. R., Abedin, K.M. and Rahman, S.M.M., "High Spatial-Resolution Digital Phase-Stepping Shearography," J. Imaging, 7, 192 (2021).
[15] Al Jabri, A. R., Abedin, K.M. and Rahman, S.M.M., "The Nyquist criterion and it relevance in phase-stepping shearography: a quantitative study, " J. Modern Opt. 69, 804-810 (2022).
[16] Anisimov, A. G., Serikova, M. G., & Groves, R. M. (2019). 3D shape shearography technique for surface strain measurement of free-form objects. Applied Optics, 58(3), 498-508